

# A simple approximation for fluids with narrow attractive potentials

D. Pini

*Istituto Nazionale per la Fisica della Materia and Dipartimento di Fisica,  
Università di Milano, Via Celoria 16, 20133 Milano, Italy*

A. Parola

*Istituto Nazionale per la Fisica della Materia and Dipartimento di Scienze Fisiche,  
Università dell'Insubria, Via Valleggio 11, 22100 Como, Italy*

L. Reatto

*Istituto Nazionale per la Fisica della Materia and Dipartimento di Fisica,  
Università di Milano, Via Celoria 16, 20133 Milano, Italy*

We study a simple modification of the optimized random phase approximation (ORPA) aimed at improving the performance of the theory for interactions with a narrow attractive well by taking into account contributions to the direct correlation function non-linear in the interaction. The theory is applied to a hard-core Yukawa and a square-well potential. Results for the equation of state, the correlations, and the critical point have been obtained for attractions of several ranges, and compared with Monte Carlo simulations. When the attractive interaction is narrow, the modified ORPA significantly improves over the plain one, especially with regard to the consistency between different routes to the thermodynamics, the two-body correlation function, and the critical temperature. However, while the spinodal curve of the modified theory is accessible, the liquid-vapor coexistence curve is not. A possible strategy to overcome this drawback is suggested.

## I. THE CLOSURE

In the last years there has been a considerable interest in model fluids in which a hard-core or very steep repulsion in the interparticle potential is followed by a narrow and deep attractive well. This interest mainly stems from the fact that such potentials provide a modelization of the interaction in many colloidal suspensions and protein solutions which, albeit crude, succeeds nevertheless in capturing the most important features of thermodynamics [1], structure [2], and phase behavior [3,4] of these systems. When describing the properties of fluids with narrow attractive potentials, it appears that the second virial coefficient plays an important role. In particular, while the critical temperature  $T_c$  depends very sensitively on the interaction range, the second virial coefficient  $B_2$  evaluated at  $T_c$  changes quite slowly [5]. Remarkably, this remains true even when considering different interaction profiles, e.g. switching from a square-well to an attractive Yukawa potential. On the basis of simulation results,  $B_2(T_c)$  is found to lie in the neighborhood of  $B_2(T_c) \simeq -6s_0$  [5], where  $s_0 = \pi\sigma^3/6$  is the volume of the particle, represented as a hard sphere of diameter  $\sigma$ . Other properties of fluids with short-range attractions exhibit a considerable degree of universality when described in terms of  $B_2$ . For instance, the range of the potential itself can be defined as that of an “equivalent” square-well fluid with the same value of  $B_2$  as the original interaction [6]. With this prescription, the disappearance of a stable liquid-vapor transition characteristic of short-ranged attractive potentials [3,4,7–9] has been found to occur at about the same range for several different interactions. It has also been observed that  $B_2$  is a relevant parameter in protein crystallization, the optimal conditions for crystallization corresponding to a narrow range of values of  $B_2$  [10].

Probably the most widespread method to model narrow attractive interactions in colloidal systems makes use of Baxter’s exact solution of the adhesive hard sphere (AHS) model [11] within the Percus-Yevick (PY) integral equation. As it is well known, this can be thought of as a square-well fluid in the limit of vanishing range and infinite well depth so that  $B_2$  will stay finite. Therefore, the relevance of the second virial coefficient in this model stems from the fact that this is the quantity which allows one to make contact with the real system. It is worthwhile recalling that the existence of an equilibrium solution for the AHS model is a consequence of the approximate character of the PY theory. In fact, it has been pointed out [12] that the AHS model is in itself thermodynamically unstable. While Baxter’s solution is successful in describing many properties of systems with very short-ranged attractive potentials, one would also like to describe these systems without resorting to the sticky limit. It is well known that the most popular perturbative approaches in liquid-state theory, such as the mean spherical approximation (MSA) and the optimized random phase approximation (ORPA) [13] are not suited for short-ranged interactions. The reason is that both of these theories

assume that the direct correlation function  $c(r)$  outside the repulsive core is simply proportional to the interaction  $w(r)$ . This is a sound assumption whenever  $w(r)$  is long-ranged, but becomes less and less so as the range of  $w(r)$  decreases to a small fraction of the size of the particles. An accurate description of the correlations is provided by other integral-equation approaches, the most successful of which is probably the modified hypernetted chain (MHNC) theory [14], in which  $c(r)$  depends on the interaction both directly and via the distribution function  $g(r)$ . On the other hand, determining the critical point by these more sophisticated methods proves difficult or even impossible, while this is accomplished quite easily within the simpler perturbative schemes. Therefore, it can be interesting to seek for a modification of the ORPA which maintains the simplicity of the original formulation, while accounting more accurately for the effects on  $c(r)$  non-linear in the interaction. This could prove useful also in the context of more complex theories, namely the renormalization-group based hierarchical reference theory (HRT) [15] and the self-consistent Ornstein-Zernike approximation (SCOZA) [16], both of which adopt a simple ORPA-like functional form for  $c(r)$ . These theories deliver the best results for the critical point and the liquid-vapor coexistence curve of simple fluids, but the inadequacy of ORPA for very short-ranged interactions partly affects their accuracy in this regime, especially as far as the correlations are concerned [17].

A possible way to modify the ORPA is suggested by the aforementioned observation that the second virial coefficient evaluated at the critical temperature depends little on the specific form of the interaction. For a potential  $v(r)$  which is the sum of a hard-core contribution and an attractive tail  $w(r)$ , this behavior could be accounted for, at the mean-field level, by replacing the usual random phase approximation (RPA) for the direct correlation function  $c(r)$

$$c(r) = c_{\text{HS}}(r) - \beta w(r) \quad (1)$$

by the expression

$$c(r) = c_{\text{HS}}(r) + e^{-\beta w(r)} - 1, \quad (2)$$

where  $\beta = 1/k_{\text{B}}T$  is the inverse temperature and  $c_{\text{HS}}(r)$  is the direct correlation function of the hard-sphere reference fluid. The latter can be considered as a known quantity, for instance by resorting to the accurate Verlet-Weis parameterization [18]. Eq. (2) corresponds to a mean-field or van der Waals-like expression for the Helmholtz free energy per unit volume  $a$ :

$$\beta a = \beta a_{\text{HS}} + \frac{1}{2} \rho^2 \int d^3 \mathbf{r} [1 - e^{-\beta w(r)}], \quad (3)$$

where  $a_{\text{HS}}$  is the Helmholtz free energy per unit volume of the hard-sphere reference fluid. As is readily seen from this expression, the mean-field critical density  $\rho_c$  does not depend on the attractive interaction  $w(r)$  and is given by  $\rho_c = 0.249\sigma^{-3}$  if the Carnahan-Starling expression [13] for the reduced compressibility of the hard-sphere gas  $\chi_{\text{red}}^{\text{HS}}(\rho)$  is used. As a consequence, Eq. (3) gives a universal value for  $B_2(T_c)$  at the critical point:

$$B_2(T_c) = \frac{1}{2} \int d^3 \mathbf{r} [1 - e^{-\beta_c v(r)}] = \frac{2}{3} \pi \sigma^3 - \frac{1}{2\rho_c \chi_{\text{red}}^{\text{HS}}(\rho_c)} = -6.601 s_0, \quad (4)$$

where  $\beta_c$  is the inverse critical temperature. This is not far from the above-mentioned value  $B_2(T_c) \simeq -6s_0$  reported in Ref. [5]. We have then considered a similar modification of the ORPA by replacing the perturbation  $-\beta w(r)$  with the Mayer function  $e^{-\beta w(r)} - 1$ . We will refer to this approximation as non-linear ORPA. The Ornstein-Zernike equation which relates the direct correlation function  $c(r)$  to the radial distribution function  $g(r)$  is then closed by means of the following *ansatz*:

$$\begin{cases} g(r) = 0 & r < \sigma, \\ c(r) = c_{\text{HS}}(r) + e^{-\beta w(r)} - 1 & r > \sigma. \end{cases} \quad (5)$$

This closure differs from Eq. (2) inasmuch as here, as in the usual ORPA, we require  $g(r)$  to vanish inside the core because of the singular repulsion. Instead of Eq. (2) we have then:

$$c(r) = c_{\text{HS}}(r) + e^{-\beta w(r)} - 1 + \mathcal{G}(r), \quad (6)$$

where the function  $\mathcal{G}(r)$  vanishes for  $r > \sigma$ , and is determined so that the *core condition*  $g(r) = 0$  for  $r < \sigma$  is satisfied. The latter can be written via the Ornstein-Zernike equation in terms of the direct correlation function in Fourier space  $\hat{c}(k)$ :

$$\int \frac{d^3 \mathbf{k}}{(2\pi)^3} e^{i\mathbf{k}\cdot\mathbf{r}} \frac{\hat{c}(k)}{1 - \rho \hat{c}(k)} = -1, \quad r < \sigma. \quad (7)$$

As is customary in ORPA calculations, we have implemented this condition in an approximate fashion by representing  $\mathcal{G}(r)$  for  $r < \sigma$  on a finite set of basis functions as a polynomial of given (typically, fourth) degree:

$$\mathcal{G}(r) = \sum_{j=1}^n u_j r^{j-1}, \quad r < \sigma. \quad (8)$$

The state-dependent coefficients  $u_j$ ,  $j = 1 \dots n$ , are determined by projecting Eq. (7) on each basis function in the interval  $0 < r < \sigma$ . If we set:

$$P_j(r) = \begin{cases} r^{j-1} & r < \sigma, \\ 0 & r > \sigma \end{cases} \quad (9)$$

and we indicate by  $f(r)$  the Mayer function  $e^{-\beta w(r)} - 1$ , Eq. (7) gives the following set of  $n$  non-linear equations for the  $n$  coefficients  $u_j$ :

$$\int \frac{d^3 \mathbf{k}}{(2\pi)^3} \hat{P}_l(k) \frac{\hat{c}_{\text{HS}}(k) + \hat{f}(k) + \sum_{j=1}^n u_j \hat{P}_j(k)}{1 - \rho [\hat{c}_{\text{HS}}(k) + \hat{f}(k) + \sum_{j=1}^n u_j \hat{P}_j(k)]} = -\hat{P}_l(k=0), \quad l = 1 \dots n, \quad (10)$$

where the hat has been used to denote Fourier transform. This system has been solved numerically by means of a standard Newton-Raphson iterative algorithm. Particular care has been taken to ensure convergence of the algorithm even for states at which the compressibility of the system is large, i.e. such that the denominator of the integrand in Eqs. (7), (10) becomes small near  $k = 0$ . By evaluating analytically the contribution to the integral at small wavevector  $k$ , we could easily achieve convergence for reduced compressibilities as large as  $\sim 10^8$ . This enabled us to accurately locate the compressibility-route critical point and the spinodal curve (that is, the locus of diverging compressibility) predicted by the theory. In order to check the reliability of the approximate procedure adopted to solve Eq. (7), we used the same method to solve the MSA for a hard-sphere fluid with an attractive Yukawa tail and compared the result with the exact solution of the MSA for this particular potential [19]. The MSA is obtained from Eq. (6) by using for  $c_{\text{HS}}(r)$  the solution of the PY equation for the hard-sphere fluid and by replacing the Mayer function with the perturbation  $-\beta w(r)$ . The comparison shows that the results obtained by the procedure described above are nearly undistinguishable from those of the exact solution for all the interaction ranges investigated here. The relative error on the reduced compressibility  $\chi_{\text{red}}$  is typically of the order of  $10^{-5}$  and does not exceed few percents for  $\chi_{\text{red}}$  in the range  $10^4$ – $10^5$ , while critical temperatures coincide to within four significant figures.

## II. RESULTS

We have assessed the performance of the non-linear ORPA of Eq. (5) by comparing its predictions for the thermodynamics, the correlations, and the critical point with those of other liquid-state theories as well as simulations. Most of the results were obtained for a hard-core Yukawa fluid at several values of the interaction range. The potential has the form

$$v(r) = \begin{cases} \infty & r < \sigma, \\ -\epsilon \sigma e^{-z(r-\sigma)}/r & r > \sigma, \end{cases} \quad (11)$$

where  $z$  is the inverse-range parameter. We also performed some calculations for a hard-core square-well potential

$$v(r) = \begin{cases} \infty & r < \sigma, \\ -\epsilon & \sigma < r < (1 + \delta) \sigma, \\ 0 & r > (1 + \delta) \sigma, \end{cases} \quad (12)$$

where  $\delta$  measures the width of the attractive well. It is worthwhile observing that for this particular potential the closure (5) amounts to evaluating the plain ORPA at an “effective” inverse temperature  $\beta_{\text{eff}}$  given by  $\beta_{\text{eff}} \epsilon = e^{\beta \epsilon} - 1$ . This corresponds to rescaling the amplitude of the perturbation  $-\beta w(r)$  so that the second virial coefficient is correctly reproduced. Such a prescription was in fact adopted several years ago to improve the performance of the MSA for the very narrow square-well potentials used to model the structure factor of microemulsions [20]. We also recall that the above interactions can be used to mimic a Lennard-Jones (LJ) fluid by suitably adjusting their ranges. Adequate values for this purpose are  $z = 1.8\sigma^{-1}$  [21] for the hard-core Yukawa potential (11) and  $\delta = 0.5$  for the square-well potential (12). In the following we will deal with substantially shorter-ranged interactions.

In figures 1–3 we report the results for the equation of state of the hard-core Yukawa fluid. Reduced temperatures  $T^* = k_B T / \epsilon$  and densities  $\rho^* = \rho \sigma^3$  will be used throughout. We have considered both the linear and the non-linear ORPA, and have compared them with the MHNC [17] and Monte Carlo (MC) simulations [17,22]. In order to determine the degree of thermodynamic consistency, results were obtained by all the three usual routes to thermodynamics, namely the compressibility, the virial, and the energy route. We recall that these are different prescriptions to obtain the thermodynamics from the two-body correlations. Specifically, in the compressibility route the key to the thermodynamics is the reduced compressibility  $\chi_{\text{red}}$  determined as the structure factor  $S(k)$  at zero wavevector  $k$ . In terms of the direct correlation function  $c(r)$ ,  $\chi_{\text{red}}$  is then given by

$$\frac{1}{\chi_{\text{red}}} = 1 - 4\pi\rho \int_0^\infty dr r^2 c(r). \quad (13)$$

In the internal energy route, the starting point to determine the thermodynamics is instead the excess internal energy per particle  $u$ , obtained by the integral of the interaction weighted by the radial distribution function  $g(r)$ :

$$u = 2\pi\rho \int_\sigma^\infty dr r^2 g(r) w(r). \quad (14)$$

Finally in the virial route the thermodynamics is obtained from the pressure  $P$  as given by the virial theorem:

$$\frac{\beta P}{\rho} = 1 + \frac{2}{3}\pi\rho \left[ \sigma^3 g(\sigma^+) - \beta \int_\sigma^\infty dr r^3 g(r) \frac{dw}{dr}(r) \right], \quad (15)$$

where the contact value of the radial distribution function  $g(\sigma^+)$  appears because of the discontinuity of the hard-core plus tail interaction considered here. While in an exact treatment Eqs. (13), (14), (15) are obviously bound to give equivalent results, this is in general not true as soon as approximations are introduced. The extent to which the equations of state determined via the various routes differ from one another is a useful test of the reliability of the theory. Figures 1–3 show that the non-linear ORPA is much more consistent than the plain ORPA, especially for short-ranged interactions. It is known [23] that for the plain ORPA the internal energy route delivers the most reliable results for the equation of state. This is true for the non-linear ORPA as well. The internal energy equations of state are actually very similar in the two cases, although for short-ranged potentials and at low temperature (see figure 3) the non-linear theory appears to be slightly superior. It is worthwhile observing that, while in the linear ORPA the pressure  $P_{\text{en}}$  obtained via the internal energy route always lies between the compressibility pressure  $P_{\text{comp}}$  and the virial one  $P_{\text{vir}}$  with  $P_{\text{vir}} < P_{\text{en}} < P_{\text{comp}}$ , this is not always the case with the non-linear ORPA. For instance, for an inverse interaction range  $z = 9\sigma^{-1}$  and reduced temperature  $T^* = 0.8$  the non-linear ORPA has again  $P_{\text{vir}} < P_{\text{en}} < P_{\text{comp}}$  (see figure 2), while for the same value of  $z$  and  $T^* = 0.45$  it gives  $P_{\text{comp}} < P_{\text{en}} < P_{\text{vir}}$  (see figure 3). For short-ranged interactions the energy-route equation of state is more accurate than the MHNC, which underestimates the simulation data.

The radial distribution function  $g(r)$  and the direct correlation function  $c(r)$  of the hard-core Yukawa fluid for several thermodynamic states and interaction ranges are shown in figures 4–6. Again, the results obtained by the linear and non-linear ORPA have been compared with the predictions of MHNC, which is known to describe two-body correlations quite accurately. For  $g(r)$ , MC simulation data [17] have also been reported. As anticipated, the plain ORPA appears to be inadequate to describe the correlations for short-ranged interactions. In particular, the contact value of  $g(r)$  is severely underestimated, with a relative error easily reaching 100%, and overall the profile of  $g(r)$  does not show enough structure. The non-linear ORPA performs considerably better by comparison, although some discrepancies with the MC data emerge, especially at low temperature and high density. These go in the opposite direction with respect to the linear ORPA, the contact value being overestimated, and the structure being somewhat overemphasized. As a consequence, as shown in the figures, the exact  $g(r)$  lies between the linear and non-linear ORPA results. Hence one expects that an accurate representation of the correlations can be obtained by performing a weighted average of the two closures. Such an approach has in fact been proposed by other authors [24] and referred to as tail interpolation method (TIM). For a hard-core plus tail potential, this consists in writing the contribution of the tail interaction to the direct correlation function outside the repulsive core as  $c(r) - c_{\text{HS}}(r) = \alpha[e^{-\beta w(r)} - 1] + (1 - \alpha)[- \beta w(r)]$ , where the parameter  $\alpha$  is determined as a function of temperature and density by imposing consistency between the virial and the compressibility routes. In Ref. [24] this method was applied to the hard-core Yukawa potential with  $z = 1.8\sigma^{-1}$  as well as the Lennard-Jones potential via the Weeks-Chandler-Andersen [25] splitting of the interaction, and very accurate results for  $g(r)$  were obtained. It could then be interesting to apply TIM also to narrower potentials. The possibility of improving the performance of the closure studied here by embedding it into a thermodynamically self-consistent scheme is discussed at the end of this section.

We observe that, unlike the linear ORPA, the non-linear closure (5) becomes exact at low density  $\rho$ , as it yields the correct zeroth-order term of the expansion of  $c(r)$  in powers of  $\rho$ , thereby giving  $c(r) \sim e^{-\beta v(r)} - 1$ ,  $g(r) \sim e^{-\beta v(r)}$  for  $\rho \rightarrow 0$ . This also implies that the second virial coefficient is correctly reproduced. Actually, it has been observed [26] that for short-ranged interactions the form  $g(r) \sim e^{-\beta v(r)}$  remains reasonably accurate near contact in a remarkably wide density interval. This is true in particular in the regime in which the fluid-solid equilibrium curve broadens up and pre-empts the gas-liquid transition. Figure 7 shows the contact values of  $g(r)$  as predicted by non-linear ORPA, MHNC, and MC simulations for the fluid with  $z = 9\sigma^{-1}$  and  $T^* = 0.4$  as a function of density. According to simulation studies [9], the states shown in the figure are well inside the fluid-solid coexistence region. The contact value of  $g(r)$  given by the non-linear ORPA is indeed very close to the value  $e^{-1/T^*} \simeq 12.18$  for densities as high as  $\rho^* = 0.8$ . The insensitivity of the peak of  $g(r)$  to the density is due to the fact that the clustering of the particles near contact is triggered by the nearly sticky attractive interaction [26]. This sharply contrasts the situation found in Lennard-Jones-like systems away from the critical point, where the structure is mainly determined by the excluded volume effect, hence being essentially that of a hard-sphere fluid at the same density.

We now turn our attention to the critical point. We have obtained critical temperatures and densities both for the hard-core Yukawa potential of Eq. (11) and the square-well potential of Eq. (12). The results obtained for several interaction ranges by the compressibility and the internal energy route of the linear and non-linear ORPA have been compared with simulation results [4,27,28,31,7,9,16] in tables I and II. The longest ranges considered correspond to the above-mentioned LJ-like values  $z = 1.8\sigma^{-1}$ ,  $\delta = 0.5$  for the Yukawa and the square-well fluid respectively. The higher degree of thermodynamic consistency of the non-linear ORPA is evident from the better agreement between energy- and compressibility-route critical temperatures with respect to the linear ORPA. In particular, the energy-route critical temperature of the non-linear ORPA is in quite good agreement with the simulation results in the whole range interval considered, although a precise assessment of the accuracy of the theory in this respect is prevented by the rather large uncertainties that usually affect critical point estimates based on simulations, as is apparent from the discrepancies between the simulation results reported in table II. The most reliable results are obtained by supplementing simulations with a finite-size scaling analysis; however, to our knowledge this was performed only for the longest ranges among those reported in the tables [16,29,31]. It is clear in any case that the compressibility route of linear ORPA gives the worst predictions, by severely underestimating the critical temperature as the interaction range decreases. For the critical density  $\rho_c$  the non-linear ORPA performs less accurately than for  $T_c$ : the compressibility route overestimates  $\rho_c$  with respect to simulation, while the energy route underestimates it. According to what observed above, for the square-well fluid the compressibility-route reduced critical temperatures  $T_{c,1}^*$  and  $T_{c,nl}^*$  predicted respectively by the linear and non-linear ORPA are linked by the relation  $1/T_{c,1}^* = e^{1/T_{c,nl}^*} - 1$ . However, this relation does not hold for the critical temperatures given by the internal energy route.

Since in introducing the closure (5) we were inspired by the empirically observed behavior of the second virial coefficient at the critical temperature, it is worthwhile considering the results for  $B_2(T_c)$  given by the theory. These have also been reported in the tables. Moreover, in figure 8 we have plotted the reciprocal of the critical temperature of the square-well fluid as a function of the logarithm of the inverse well width  $1/\delta$ . If  $B_2(T_c)$  were rigorously independent of  $\delta$ , this plot would yield a straight line in the small- $\delta$  limit. The slow variation of  $B_2(T_c)$  with  $\delta$  gives a nearly linear dependence of  $1/T_c$  on  $\ln(1/\delta)$  in a relatively wide interval of  $\delta$ , with the non-linear ORPA closely following the simulation results. However, neither the simulation data nor the theory show evidence of  $B_2(T_c)$  saturating to a constant value in the interval considered. We observe that the linear ORPA gives rather poor results for  $B_2(T_c)$ . In particular, the values obtained via the compressibility route of linear ORPA are way too large in modulus and even show the wrong trend because of the strong underestimation of  $T_c$ .

Below the critical temperature of the compressibility route, both the linear and the non-linear ORPA give a spinodal curve, along which the compressibility given by Eq. (13) diverges. Inside the region bounded by this curve the approximation cannot be solved, as the integrand in the l.h.s. of Eq. (10) would develop a pole at non-zero wavevector and the integral would diverge. In order to obtain the coexistence curve, the problem arises of avoiding this forbidden region when determining the pressure and the chemical potential needed to impose the thermodynamic equilibrium conditions. In the linear ORPA, this is achieved via the internal energy route, namely by getting the excess Helmholtz free energy by integrating along each isochore the excess internal energy given by Eq. (14). The success of this procedure depends on the fact that, as shown in tables I, II, the critical temperature of the compressibility route of linear ORPA is considerably lower than that of the internal energy route, at least for the simple model fluids considered here. Therefore, the forbidden region lies well inside the internal energy coexistence boundary. However, we have found that this method is not effective when dealing with the non-linear ORPA. In fact, as observed above, in this case the difference between the critical temperatures given by the compressibility and the internal energy route is relatively small. As a consequence, the relative location of the energy-route critical point and the spinodal curve is such that a substantial portion of the coexistence curve should lie inside the forbidden region. This prevented us from determining the coexistence curve, save for a tiny part corresponding to the very top. The situation just described is illustrated in figure 9, which shows the spinodal curve predicted by the non-linear ORPA for a hard-core Yukawa

fluid with  $z = 4\sigma^{-1}$ , together with the locus of points at which the internal-energy route compressibility diverges. For densities just above the critical one, the latter curve bumps into the spinodal. This rapidly widens as the temperature is lowered, so that also the high-density branch of the coexistence curve is swallowed by the forbidden region. Such a feature is clearly quite a serious limitation of the non-linear ORPA, especially since the thermodynamic consistency of the theory is not so high as to allow one to reliably determine the pressure and the chemical potential along a mixed integration path in the temperature-density plane, as it is often done with other integral-equation theories [14,30]. A possible strategy to overcome it consists in using a functional form of  $c(r)$  similar to that considered here in the context of a more sophisticated theory, such as the SCOZA or the HRT mentioned in the previous section. This could be accomplished by multiplying the Mayer function in Eqs. (5), (6) by a state-dependent amplitude  $A(\rho, T)$ . In the SCOZA  $A(\rho, T)$  is determined by imposing consistency between the compressibility and the energy route, while in the HRT one requires the compressibility rule (13) to be satisfied along a process in which the Helmholtz free energy of the system is obtained by gradually switching on the long-wavelength Fourier components of the interaction. Both of these procedures are expected to lead to a well-defined coexistence curve. In fact, in the SCOZA the spinodal curve and the curve along which the internal-energy route compressibility diverges are forced to coincide. Since the coexistence boundary lies outside the latter curve, it will lie outside the forbidden region as well. On the other hand the HRT, thanks to its renormalization-group structure, preserves the convexity of the free energy for every thermodynamic state. No forbidden region appears, and the two-phase domain is correctly obtained as the locus of flat pressure-density isotherms [15]. As stated above, the accuracy of both the SCOZA and the HRT for short-ranged interactions is affected by the functional form adopted for  $c(r)$ , similar to that of the linear ORPA. The predictions for  $c(r)$  given by the linear and non-linear ORPA for a number of different states of the Yukawa fluid have already been compared to the accurate MHNC results in figures 4–6. In figure 10 the direct correlation function outside the repulsive core for the Yukawa fluid with  $z = 9\sigma^{-1}$ ,  $T^* = 0.4$ ,  $\rho^* = 0.8$  shown in figure 6 has been rescaled by its value at contact  $c(\sigma^+)$ . It appears that, even when both the linear and the non-linear ORPA differ considerably from the MHNC as for the state considered here, the overall profile of  $c(r)$  given by the non-linear ORPA can be adjusted so as to reproduce that of the MHNC fairly well by suitably rescaling its amplitude, while this is not the case with the linear theory. Accordingly, we expect that implementing a closure similar to that of Eq. (6) within the HRT or the SCOZA scheme along the lines sketched above will lead to an accurate description of thermodynamics, correlations, and phase diagram of fluids with narrow attractive potentials. We intend to pursue this investigation in the future.

### III. CONCLUSIONS

We have considered a simple modification of the ORPA aimed at improving the performance of this theory for interactions which present a narrow and deep attractive well. Its predictions have been compared with those of linear ORPA and MHNC as well as simulation data. The equation of state is accurately reproduced, and the degree of thermodynamic consistency is considerably higher than in the plain ORPA. Also the two-body correlations are more accurate than those of plain ORPA, although overall less accurate than in MHNC. The critical temperatures agree well with simulation results. In particular, the second virial coefficient at the critical temperature  $B_2(T_c)$  is found to depend rather weakly on the interaction range. Below the critical temperature the spinodal curve predicted by the theory can be easily obtained, but unfortunately most of the liquid-vapor coexistence curve is not accessible, as it lies inside the region where no solutions can be found. This drawback could be overcome by using a functional form of the direct correlation function similar to that considered here in the context of a more sophisticated approach such as the HRT or the SCOZA.

### ACKNOWLEDGMENTS

We thank Dino Costa and Giuseppe Pellicane for making available to us the files of their MC and MHNC results and their MHNC code.

- 
- [1] Piazza, R., 1999, *J. Crystal Growth* **196**, 415.
- [2] Malfois, M., Bonneté, F., Belloni, L., and Tardieu, A., 1996, *J. Chem. Phys.* **105**, 3290.
- [3] Rosenbaum, D., Zamora, P. C., and Zukoski, C. F., 1996, *Phys. Rev. Lett* **76**, 150.
- [4] Lomakin, A., Asherie, N., and Benedek, G. B., 1996, *J. Chem. Phys.* **104**, 1646.
- [5] Vliegthart, G. A., and Lekkerkerker, H. N.W., 2000, *J. Chem. Phys.* **112**, 5364.
- [6] Noro, M. G., and Frenkel, D., 2000, *J. Chem. Phys.* **113**, 2941.
- [7] Lomba, E., and Almarza, N. G., 1994, *J. Chem. Phys.* **100**, 8367.
- [8] Mederos, L., and Navascués, G., 1994, *J. Chem. Phys.* **101**, 9841.
- [9] Hagen, M. H. J., and Frenkel, D., 1994, *J. Chem. Phys.* **101**, 4093.
- [10] George, A., and Wilson, W. W., 1994, *Acta Cryst. D* **50**, 361.
- [11] Baxter, R. J., 1968, *J. Chem. Phys.* **49**, 2770.
- [12] Stell, G., 1991, *J. Stat. Phys.* **63**, 1203.
- [13] See, for instance, Hansen, J. P., and McDonald, I. R., 1986, *Theory of Simple Liquids* (London: Academic Press).
- [14] See, for instance, Caccamo, C., 1996, *Phys. Rep.* **274**, 1.
- [15] Parola, A., and Reatto, L., 1995, *Adv. Phys.* **44**, 211.
- [16] Pini, D., Stell, G., and Wilding, N. B., 1998, *Mol. Phys.* **95**, 483.
- [17] Caccamo, C., Pellicane, G., Costa, D., Pini, D., and Stell, G., 1999, *Phys. Rev. E* **60**, 5533; Costa, D., and Pellicane, G., private communication.
- [18] Verlet, L., and Weis, J. J., 1972, *Phys. Rev. A* **5**, 939; Henderson, D., and Grundke, E. W., 1975, *J. Chem. Phys.* **63**, 601.
- [19] Waisman, E., 1973, *Mol. Phys.* **25**, 45; Høye, J. S., and Stell, G., 1976, *Mol. Phys.* **32**, 195.
- [20] Huang, J. S., Safran, S. A., Kim, M. W., Grest, G. S., Kotlarchyk, M., and Quirke, N., 1984, *Phys. Rev. Lett* **53**, 592.
- [21] Henderson, D., Waisman, E., Lebowitz, J. L., and Blum, L., 1978, *Mol. Phys.* **35**, 241.
- [22] Shukla, K. P., 2000, *J. Chem. Phys.* **112**, 10358.
- [23] Konior, J., 1989, *Mol. Phys.* **68**, 129.
- [24] Katsov, K., and Weeks, J. D., 2000, *J. Stat. Phys.* **100**, 107.
- [25] Weeks, J. D., Chandler, D., and Andersen, H. C., 1971, *J. Chem. Phys.* **54**, 5237.
- [26] Louis, A. A., 2001, *Phil. Trans. R. Soc. Lond. A* **359**, 939.
- [27] Vega, L., de Miguel, E., Rull, L. F., Jackson, G., and McLure, I. A., 1992, *J. Chem. Phys.* **96**, 2296.
- [28] Elliott, J. R., and Hu, L., 1999, *J. Chem. Phys.* **110**, 3043.
- [29] Brilliantov, N. V., and Valleau, J. P., 1998, *J. Chem. Phys.* **108**, 1123.
- [30] Caccamo, C., Giunta, G., and Malescio, G., 1995, *Mol. Phys.* **84**, 125.
- [31] Orkoulas, G., and Panagiotopoulos, A. Z., 1999, *J. Chem. Phys.* **110**, 1581.

	z=1.8			z=3			z=4			z=7		
	$T_c^*$	$\rho_c^*$	$B_2(T_c)$									
MC1	1.212	0.312	-5.90									
MC2	1.177	0.313	-6.24	0.715	0.375	-6.14	0.576	0.377	-5.92			
MC3										0.412	0.50	-5.51
ORPA (comp)	1.037	0.312	-7.89	0.542	0.360	-11.10	0.387	0.392	-15.35	0.213	0.460	-46.70
ORPA (energy)	1.243	0.318	-5.61	0.771	0.374	-5.16	0.624	0.420	-4.75	0.451	0.536	-4.05
ORPANL (comp)	1.221	0.326	-5.82	0.749	0.388	-5.52	0.602	0.432	-5.29	0.430	0.504	-4.77
ORPANL (energy)	1.210	0.270	-5.92	0.736	0.302	-5.75	0.591	0.324	-5.55	0.424	0.362	-4.98

TABLE I. Critical constants of the hard-core Yukawa fluid. The reduced critical density  $\rho_c^*$  and temperature  $T_c^*$  from the compressibility and energy route of linear and non-linear ORPA (indicated as ORPANL) are compared with simulation results. The second virial coefficient at the critical temperature  $B_2(T_c)$  is in units of the hard-sphere volume  $\pi\sigma^3/6$ . MC1: Monte Carlo simulation data with finite-size scaling from Ref. [16]. MC2: Monte Carlo simulation data from Ref [7]. MC3: Monte carlo simulation data from Ref. [9].

	$\delta = 0.5$			$\delta = 0.375$			$\delta = 0.25$			$\delta = 0.1$		
	$T_c^*$	$\rho_c^*$	$B_2(T_c)$	$T_c^*$	$\rho_c^*$	$B_2(T_c)$	$T_c^*$	$\rho_c^*$	$B_2(T_c)$	$T_c^*$	$\rho_c^*$	$B_2(T_c)$
MC1	1.218	0.310	-8.09									
MC2	1.219	0.299	-8.08	0.974	0.355	-7.46	0.764	0.370	-6.30			
MC3	1.299	0.322	-7.01				0.788	0.392	-5.75	0.491	0.456	-4.82
MD	1.27	0.31	-7.38	1.01	0.34	-6.82	0.78	0.42	-5.93			
ORPA (comp)	0.881	0.348	-16.05	0.624	0.388	-21.40	0.423	0.420	-32.73	0.158	0.537	-737.88
ORPA (energy)	1.327	0.304	-6.68	1.083	0.354	-5.72	0.846	0.438	-4.61	0.529	0.686	-3.43
ORPANL (comp)	1.319	0.348	-6.78	1.045	0.388	-6.26	0.824	0.420	-5.01	0.502	0.537	-4.38
ORPANL (energy)	1.282	0.228	-7.22	1.038	0.266	-6.36	0.806	0.330	-5.37	0.497	0.450	-4.57

TABLE II. Same as table I for the square-well fluid. MC1: Monte Carlo simulation data with finite-size scaling from Ref. [31]. MC2: Monte Carlo simulation data from Ref. [27]. MC3: Monte Carlo simulation data from Ref. [4]. MD: molecular dynamics simulation data from Ref. [28].

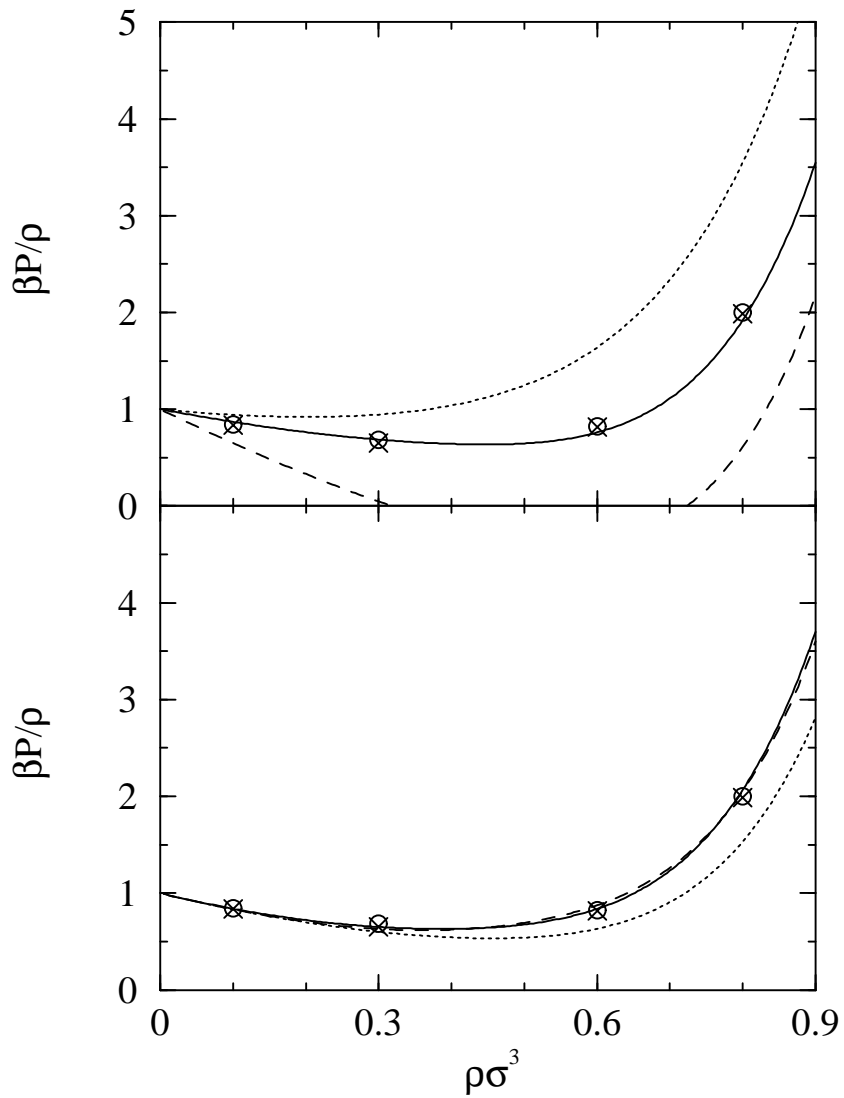


FIG. 1. Compressibility factor of the hard-core Yukawa fluid (see Eq. (11)) with inverse range  $z = 4\sigma^{-1}$  at reduced temperature  $T^* = 0.7$ , corresponding to  $T/T_c \simeq 1.2$ . The compressibility, virial, and energy routes of the linear ORPA (upper panel) and non-linear ORPA (lower panel) are compared with MHNC and MC results. Upper panel: dotted line, linear ORPA compressibility route; dashed line, linear ORPA virial route; solid line: linear ORPA energy route; crosses, MHNC; and circles, MC simulation results [22]. Lower panel: same notation as in the upper panel for the non-linear ORPA.

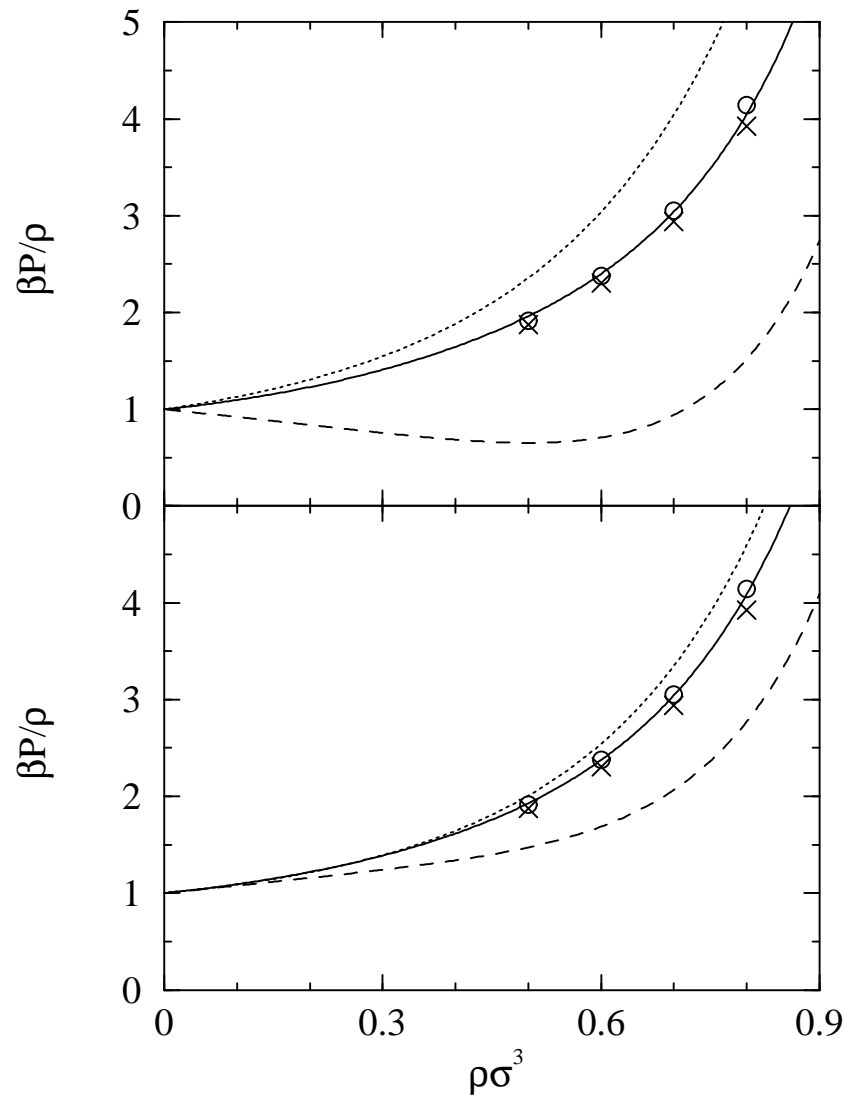


FIG. 2. Same as figure 1 with  $z = 9\sigma^{-1}$  and  $T^* = 0.8$ . MHNC and MC results are from Ref. [17].

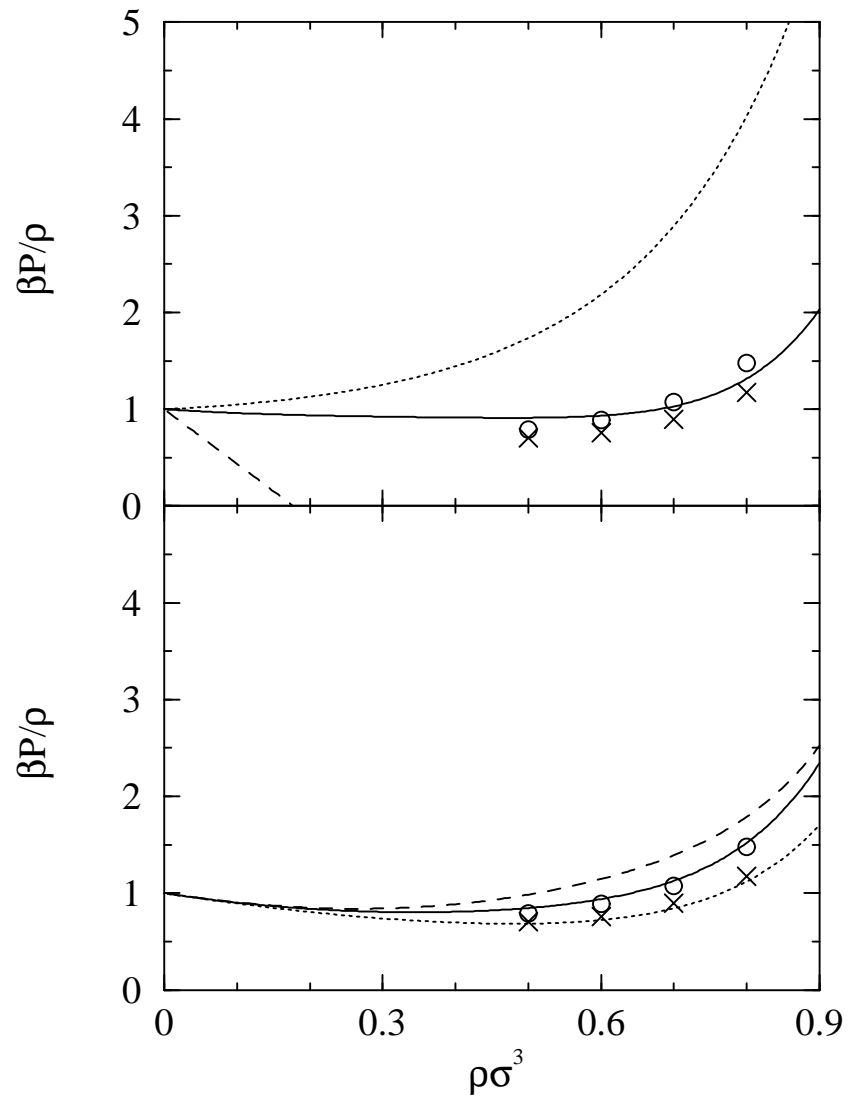


FIG. 3. Same as figure 1 with  $z = 9\sigma^{-1}$  and  $T^* = 0.45$ . MHNC and MC results are from Ref. [17].

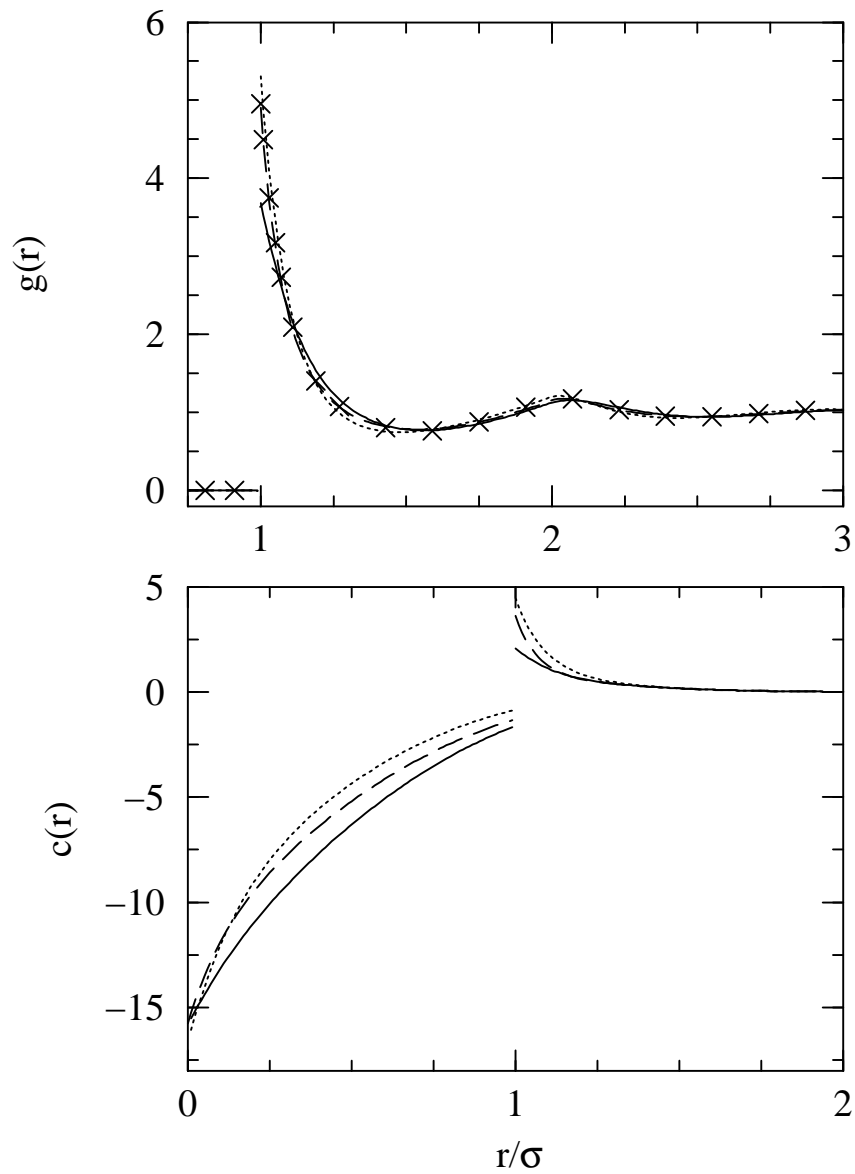


FIG. 4. Radial distribution function  $g(r)$  (upper panel) and direct correlation function  $c(r)$  (lower panel) of the hard-core Yukawa fluid with  $z = 4\sigma^{-1}$  at reduced density  $\rho^* = 0.7$  and temperature  $T^* = 0.62$ , slightly above its critical value. Solid line, linear ORPA; dotted line, non-linear ORPA; long-dashed line, MHNC; and crosses, MC data from Ref. [17].

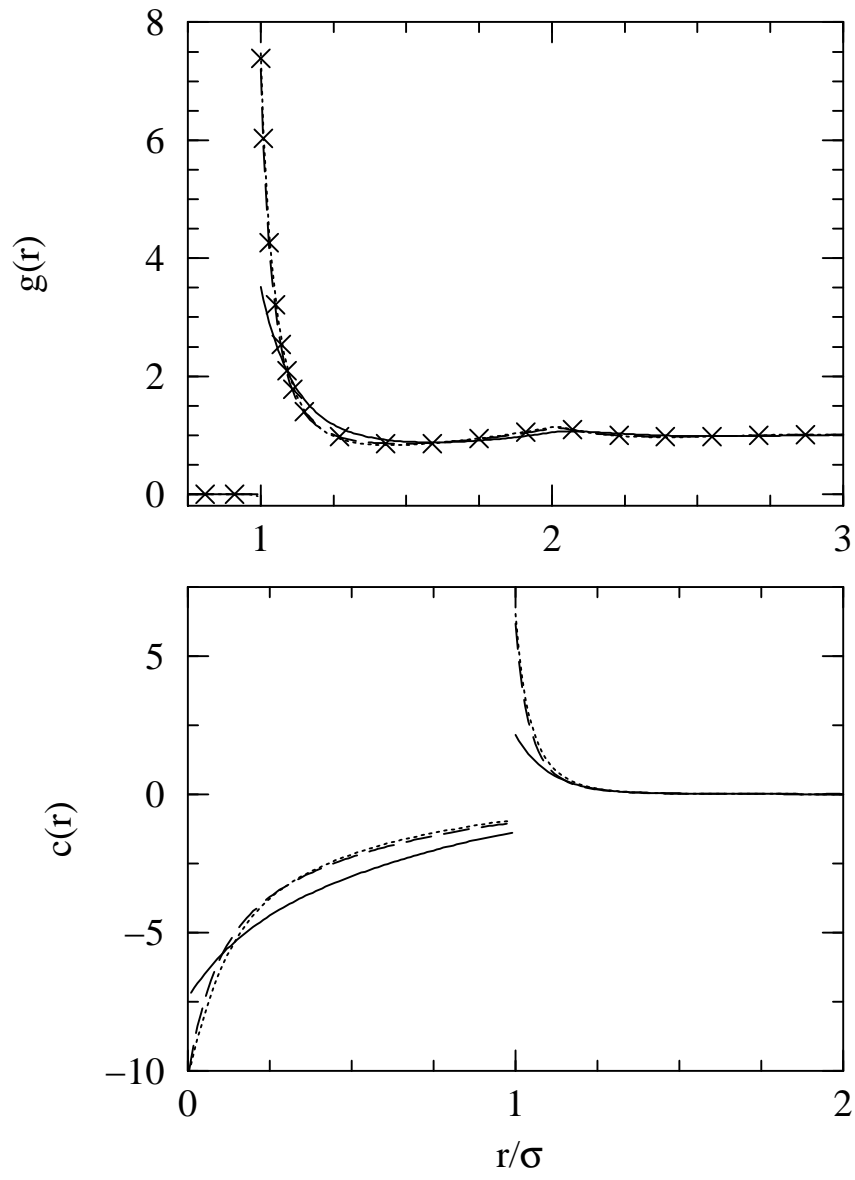


FIG. 5. Same as figure 4 for  $z = 9\sigma^{-1}$ ,  $\rho^* = 0.5$ ,  $T^* = 0.5$ . According to simulation studies [9], this state point lies somewhat above the fluid-solid line.

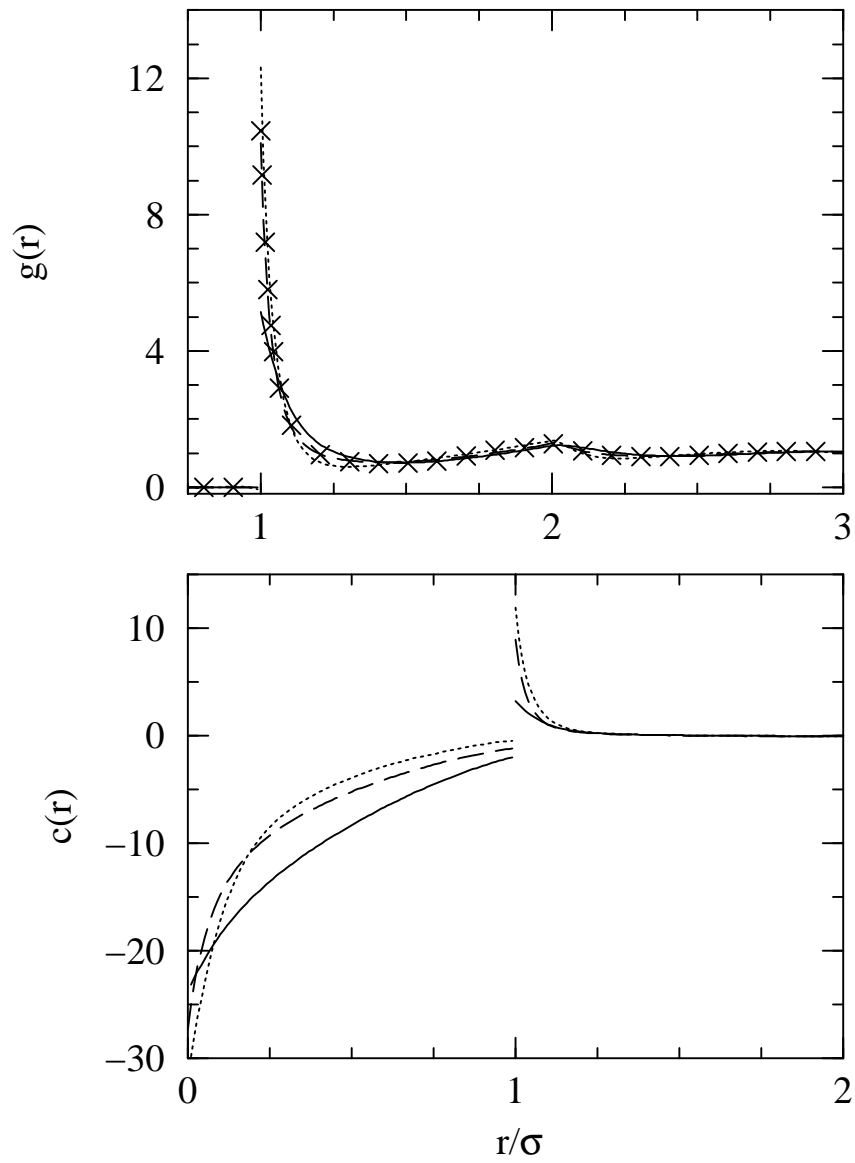


FIG. 6. Same as figure 4 for  $z = 9\sigma^{-1}$ ,  $\rho^* = 0.8$ ,  $T^* = 0.4$ . According to Ref. [9], this state point lies well inside the fluid-solid coexistence region.

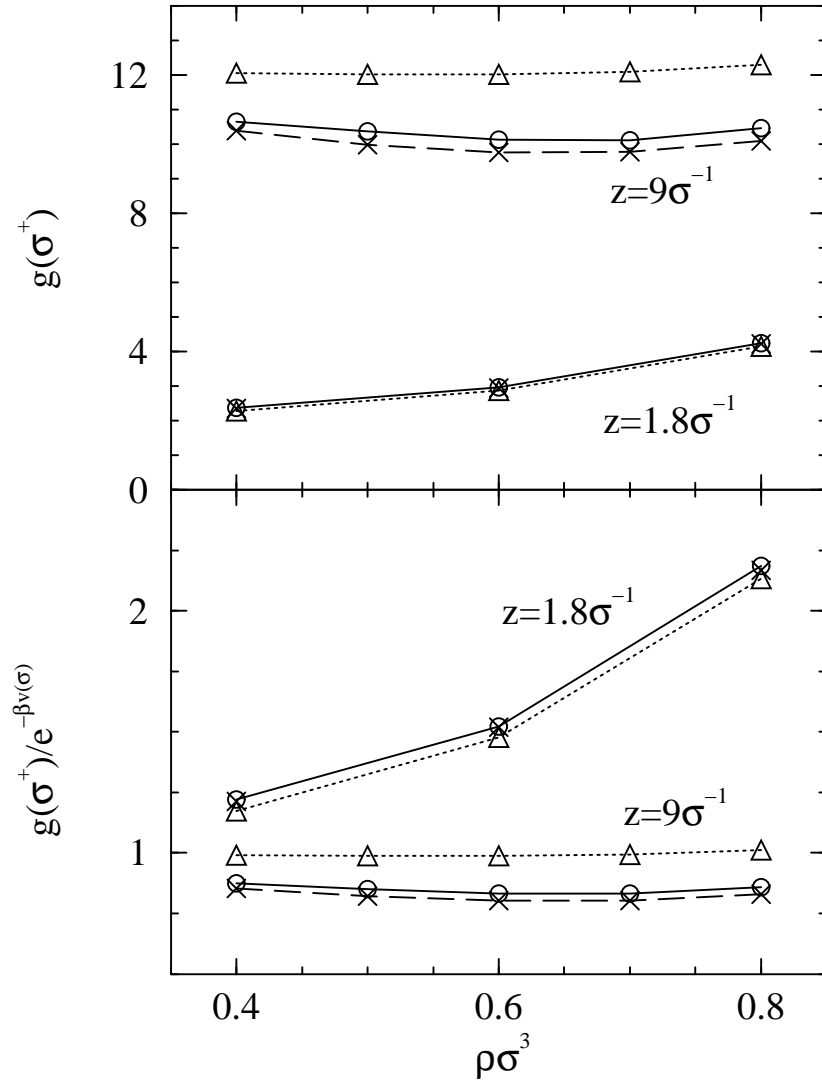


FIG. 7. Upper panel: contact value  $g(\sigma^+)$  of the radial distribution function of the hard-core Yukawa fluid with  $z = 1.8\sigma^{-1}$ ,  $T^* = 1.5$  and  $z = 9\sigma^{-1}$ ,  $T^* = 0.4$ . Both isotherms lie slightly above the critical temperature for the corresponding  $z$ . Lower panel: contact value  $g(\sigma^+)$  rescaled by its low-density limit  $e^{-\beta v(\sigma^+)}$ . Triangles, non-linear ORPA; crosses: MHNC; and circles, MC results [17]. The shorter-ranged interaction has a much larger contact value, which remains nearly constant from  $\rho^* = 0.4$  to  $\rho^* = 0.8$ . In the same interval, the contact value of the longer-ranged interaction increases by nearly a factor 2 on increasing  $\rho^*$ .

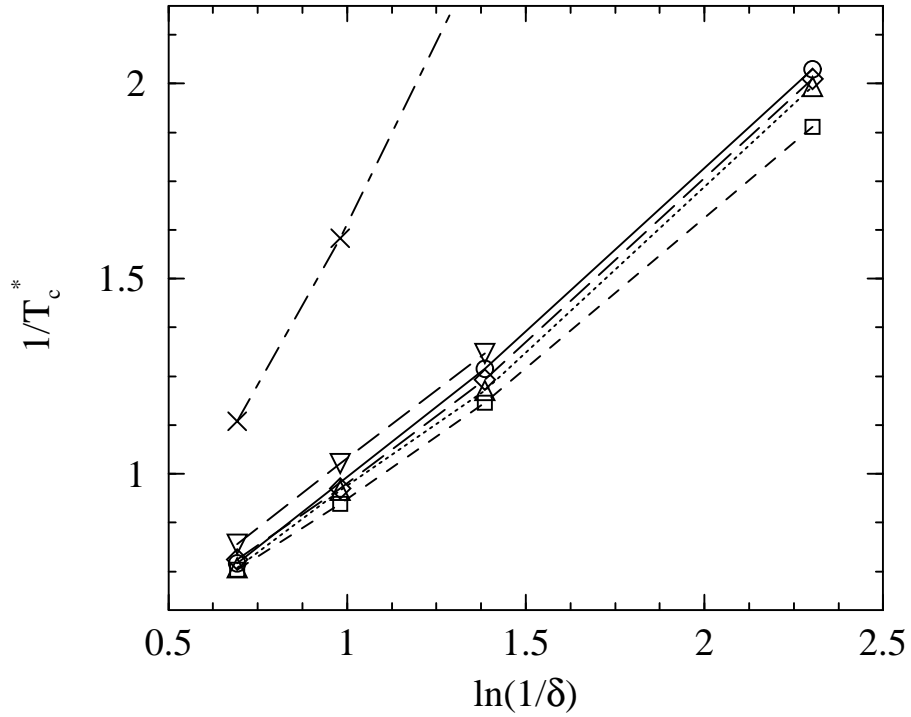


FIG. 8. Inverse reduced critical temperature  $1/T_c^*$  of the square-well fluid as a function of the width  $\delta$  of the attractive well (see Eq. (12)). The points shown correspond to  $\delta = 0.5$ ,  $\delta = 0.375$ ,  $\delta = 0.25$ , and  $\delta = 0.1$ . Crosses: linear ORPA compressibility route; squares, linear ORPA energy route; triangles, non-linear ORPA compressibility route; diamonds, non-linear ORPA energy route; circles, MC simulation data from Ref. [4]; and inverted triangles, MC simulation data from Ref. [27]. Lines are a guide for the eye. The nearly linear dependence of  $1/T_c^*$  on the logarithm of the inverse range  $1/\delta$  stems from  $B_2(T_c)$  being a slowly varying function of  $\delta$ .

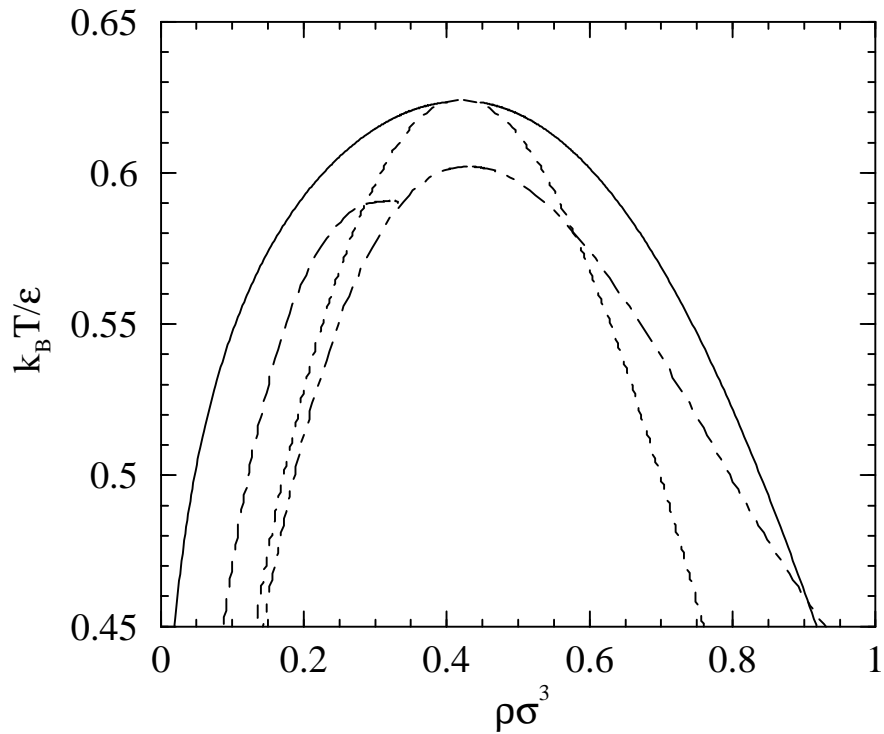


FIG. 9. Dot-dashed line, spinodal curve of the hard-core Yukawa fluid with inverse range  $z = 4\sigma^{-1}$  according to the compressibility route of non-linear ORPA. No solutions are found in the region bounded by this curve. Long-dashed line, locus of diverging compressibility according to the energy route of non-linear ORPA. Note that this curve bumps into the spinodal. Dashed line, locus of diverging compressibility according to the energy route of linear ORPA; solid line, coexistence curve according to the energy route of linear ORPA. The compressibility-route spinodal of linear ORPA lies well inside the coexistence curve and is located below the plane of the figure.

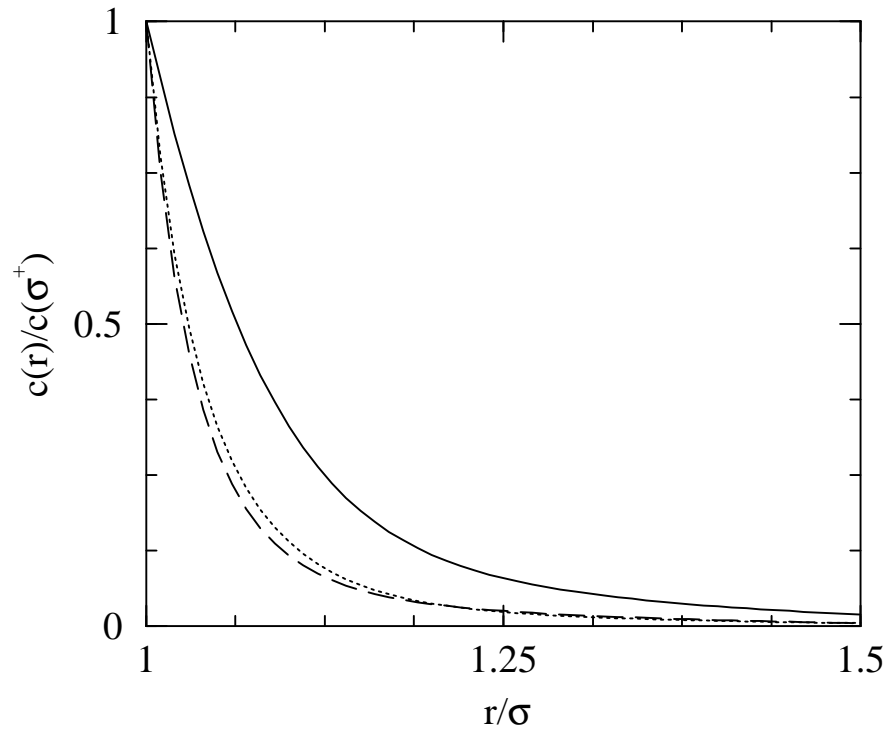


FIG. 10. Direct correlation function  $c(r)$  of the hard-core Yukawa fluid with  $z = 9\sigma^{-1}$ ,  $T^* = 0.4$ ,  $\rho^* = 0.8$ , as predicted by linear ORPA (solid line), non-linear ORPA (dotted line), and MHNC (long-dashed line), rescaled by its contact value  $c(\sigma^+)$ .